Aberration Measurement from Crystalline Ronchigrams with an Attention Neural Network

Jingrui Wei[1], and Paul M. Voyles[1*]

[1.] Department of Materials Science and Engineering, University of Wisconsin-Madison, Madison, WI, United States of America

* Corresponding author: paul.voyles@wisc.edu

It is essential to measure and compensate the aberrations of the objective lens to achieve high spatial resolution in scanning transmission electron microscopy (STEM). Precise and efficient measurement of probe aberrations facilitates live aberration correction when a crystal specimen of interest is inserted and provides better initial guess of the probe function for phase retrieval techniques like ptychography. While diagnostic methods using Ronchigrams have been proposed for crystalline specimens [1], their widespread implementation is hindered by the complexity and long acquisition time required for a focal series of Ronchigrams and adaptation to various crystal lattices. We have developed AberrationNet, a deep neural network based on a residual neural network and attention mechanism [2], which provides rapid first and second-order aberration coefficient estimation from two Ronchigrams of a zone-axis crystalline specimen at different defocus.

Figure 1a compares the Ronchigrams of the $SrTiO_3$ [001] lattice at large defocus from a perfect probe and a probe with significant aberration. Considering a three-beam condition, the Ronchigram of a thin crystal can be approximated as [1]

$$I(\boldsymbol{k}) = 4a\cos\left(\pi\lambda^{-1}\left(\chi(\boldsymbol{k}-\boldsymbol{h})-\chi(\boldsymbol{k}-\boldsymbol{g})\right)\right)\times \cos\left(\pi\lambda^{-1}\left(2\chi(\boldsymbol{k})-\chi(\boldsymbol{k}-\boldsymbol{g})-\chi(\boldsymbol{k}-\boldsymbol{h})\right)\right). \quad (1)$$

The resulting sinusoidal fringes depend on the aberration function χ as well as the two diffraction spots at angles **g** and **h,** and the fringe spacing changes across the Ronchigram at different *k*. If we consider a small patch at angle **T**, the Fourier transform of equation (1) can measure the spacing and give the coordinate of the resulting delta functions as [1]

$$S(\boldsymbol{T}) = \pm\nabla\left(\chi(\boldsymbol{T}-\boldsymbol{h})-\chi(\boldsymbol{T}-\boldsymbol{g})\right). \quad (2)$$

Thus the delta function coordinates correspond to the divergence of the aberration function and the diffraction vectors. This equation also allows determination of the diffraction vector from two Ronchigrams with known focus step [1]: $\boldsymbol{g} = (S(\boldsymbol{T})_2 - S(\boldsymbol{T})_1)/\,dC1$. Figure 1b shows the difference images between the Fourier power spectra from large underfocus Ronchigram patches (Δf = C1-400nm) and large overfocus (Δf = C1+400nm) Ronchigram patches. The displacements of the delta function spots show different magnitudes and directions due to the probe aberration.

However, real-world data with multiple beam interference modulates the fringe pattern and poses challenges for interpreting the Ronchigram. Previous studies have leveraged convolutional neural networks (CNN) to predict aberrations from amorphous Ronchigrams [3], demonstrating the potential to discern feature-aberration relationships with CNNs. We developed a deep neural network with physics-informed design to approximate the decomposition of aberration function from the Fourier transform (FT)

difference patches, ensuring robustness against variations in real experimental data through comprehensive training. The AberrationNet model is built based on the Resnet architecture and incorporates the idea of equation (2) into coordinate attention layers [4] and channel attention layers [5]. Coordinate attention highlights the position of features in the FT patches. Channel attention enhances the learning of the relationship between channels, which are the FT patches from the entire Ronchigram. Each channel serves as a sampling point of the divergence of the aberration function over the diffraction plane. AberrationNet combines two similar architectures: the first one predicts the first order aberration coefficients (C10, C12a, C12b), and the second one, using the first model prediction as additional input, predicts the second order coefficients (C21a, C21b, C23a, C23b). The two parts were trained alternatively to optimize the model performance. We utilized Cartesian coefficients as the target instead of polar coefficients to avoid incorporating periodic functions (e.g., sin and cos) in the function being approximated by the neural network.

We validated the AberrationNet with multislice simulated Ronchigrams. **Figure 2(a-c)** illustrates residual distributions for the model trained and tested on the same lattice $SrTiO_3$ [001], with accuracy metrics summarized in **Figure 2d**. AberrationNet exhibits robustness against variations in thickness, mistilt, and convergence angle within experimentally likely ranges for high-resolution zone-axis STEM imaging. The overall accuracy of the model is sufficient for diagnosis of aberration for post-processing techniques like ptychography reconstruction and potential integration into a STEM probe correction workflow.

The current AberrationNet works only for $SrTiO_3$ [001]. One path to generalizing it is automated training of a new AberrationNet on simulated Ronchigrams for other crystals. It may also be possible to develop a more advanced model which includes the lattice diffraction vectors of the zone axis as an additional model input.

This research was supported by NSF Cyberinfrastructure for Sustained Scientific Innovation (CSSI) award No. 1931298.

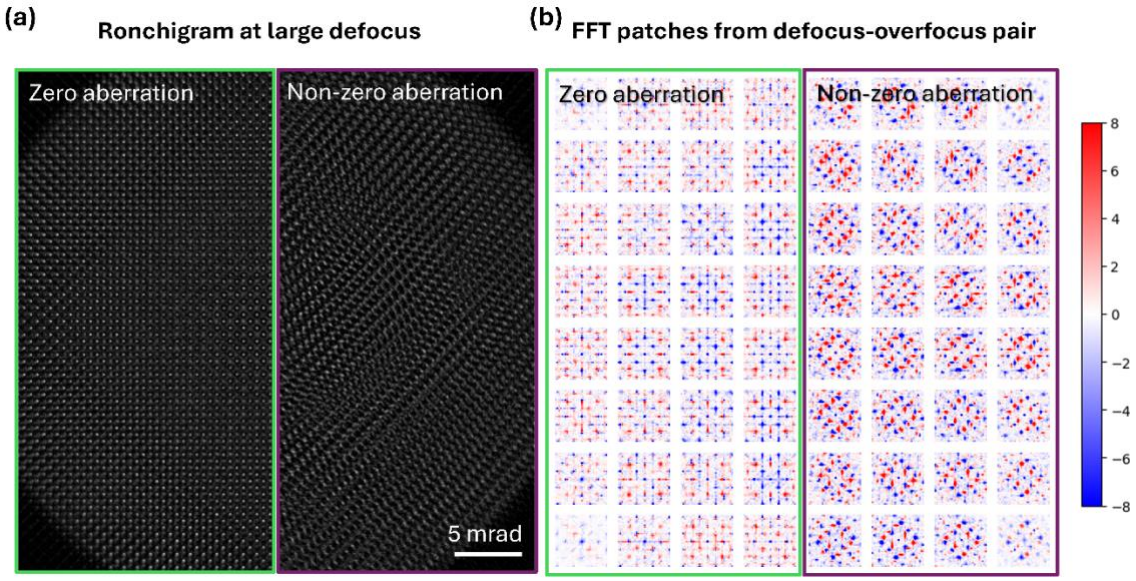

Figure 1. Effect of aberration in defocused crystalline Ronchigram and example input data for the AberrationNet model. (a) simulated Ronchigram of $SrTiO_3$ [001] with defocus ~ 400 nm, the green half is simulated using a probe of zero C12, C21, C23, etc., and the purple half is from a probe with significant aberrations. (b) difference images between Fourier power spectra from the underfocus segmented Ronchigram patches and the overfocus segmented Ronchigram patches. The green and purple outlines identify corresponding data in (a) and (b).

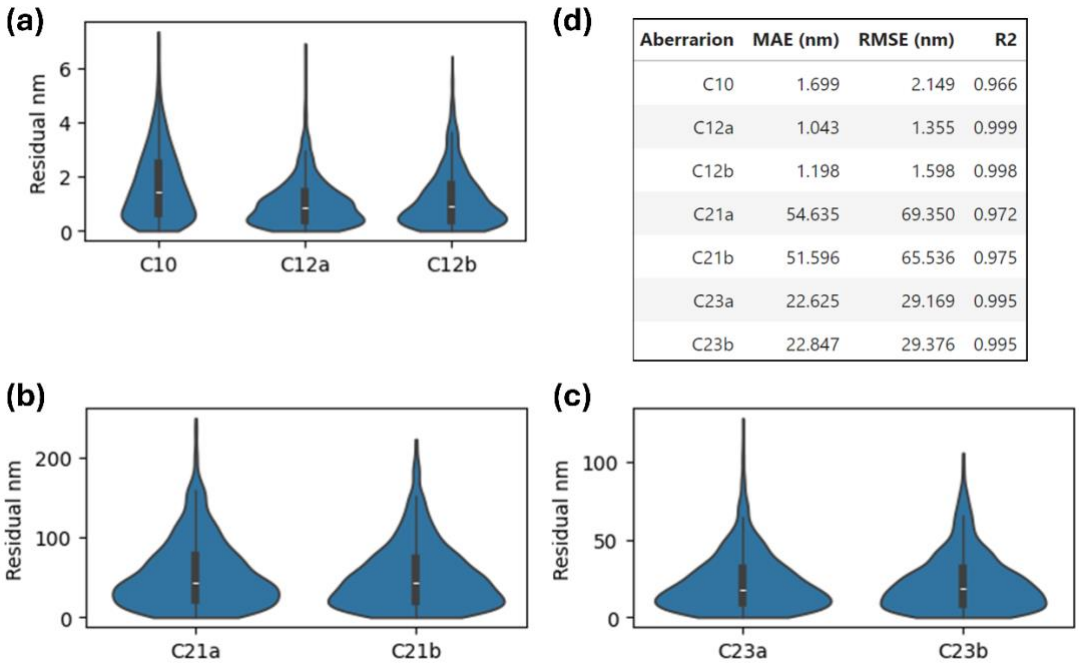

(d)

Aberrarion	MAE (nm)	RMSE (nm)	R2
C10	1.699	2.149	0.966
C12a	1.043	1.355	0.999
C12b	1.198	1.598	0.998
C21a	54.635	69.350	0.972
C21b	51.596	65.536	0.975
C23a	22.625	29.169	0.995
C23b	22.847	29.376	0.995

Figure 2. AberrationNet accuracy measurement. (a) Violin plot of the residual of first order aberration coefficients (b) the residual of C21(B2) aberration (c) the residual of C23(A2) aberration (d) summarizing the mean absolute error, root mean square error, and R2 score of the model prediction of all seven aberration coefficients.

References:

[1] A. R. Lupini and S. J. Pennycook, Journal of Electron Microscopy **57**, 6 (2008), pp. 195–201
[2] J. Hu *et al.*, Proc. IEEE Comput. Soc. Conf. Comput. Vis. Pattern Recognit. (2018), pp. 7132–7141
[3] G. Bertoni *et al.*, Ultramicroscopy, **245**, 113663 (2023)
[4] Q. Hou *et al.*, Proc. IEEE Comput. Soc. Conf. Comput. Vis. Pattern Recognit. (2021), pp. 13708–13717
[5] F. Zou *et al.*, IEEE J. Transl. Eng. Heal. Med. **11**, March (2023), pp. 252–260